Sea Ice Loss and Arctic Cyclone Activity from 1979 to 2014

Tomoko Koyama

Department of Atmospheric and Oceanic Sciences, University of Colorado Boulder, Boulder, Colorado

Julienne Stroeve

*National Snow and Ice Data Center, Cooperative Institute for Research in Environmental
Sciences, Boulder, Colorado*

John Cassano

*Cooperative Institute for Research in Environmental Sciences, and Department of Atmospheric and
Oceanic Sciences, University of Colorado Boulder, Boulder, Colorado*

Alex Crawford

*National Snow and Ice Data Center, Cooperative Institute for Research in Environmental
Sciences, Boulder, Colorado*

ABSTRACT

Extensive summer sea ice loss has occurred within the Beaufort, Chukchi, East Siberian, and Laptev Seas over the last decade. Associated anomalies in sensible and latent heat fluxes in autumn have increased Arctic atmospheric precipitable water and air temperatures, with the potential to impact autumn and winter cyclone activity. To examine if a connection exists between recent Arctic sea ice loss and cyclone activity, several cyclone metrics from 60° to 90°N are analyzed. Results show that following years with less September sea ice, there is a subsequent increase in moisture availability, regional baroclinicity, and changes in vertical stability that favor cyclogenesis. However, tracking of individual cyclones indicates no coherent increase in cyclone frequency or intensity associated with sea ice loss. Furthermore, no robust northward progression of extreme cyclones is observed.

1. Introduction

Extratropical storms transport atmospheric energy from lower latitudes into the polar regions. These cyclones initially form as waves in regions of enhanced temperature contrasts, referred to as baroclinic zones. In summer, when the central Arctic Ocean experiences a cyclone maximum (Serreze and Barrett 2008), cyclogenesis (the formation and intensification of cyclones) is particularly common over the Eurasian continent (Crawford and Serreze 2016).

Whereas Arctic cyclone formation over Eurasia peaks in the summer, the autumn and winter show a predominance of storm tracks originating in the northern North Atlantic and propagating toward the Greenland, Norwegian, and Barents Seas (e.g., Zhang et al. 2004). Shallow baroclinic zones typically found along the ice edge may provide the initial conditions for some of these storms (Tsukernik et al. 2007), which play an important role in our climate system by impacting precipitation, the radiation budget, cloudiness, and poleward heat and moisture transport (Bengtsson et al. 2006; Sorteberg and Walsh 2008). For example, at the end of December 2015, a strong cyclone entered the Arctic, transporting warm and humid air over the sea ice areas, resulting in localized thinning and retreat of sea ice (Boisvert et al. 2016).

During the last four decades, Arctic sea ice extent (SIE) has declined by more than 40% during summer

(e.g., Stroeve et al. 2012; Serreze and Stroeve 2015; Simmonds 2015), leading to large open water areas in autumn that result in stronger heat and moisture transfers from the ocean to the atmosphere: turbulent fluxes of sensible and latent heat from the ocean are increased, as is longwave radiation emitted by the sea surface (e.g., Serreze et al. 2009; Screen and Simmonds 2010a). This leads to large increases in near-surface air temperatures, which have been particularly strong in recent years during the month of October, a month after the seasonal minimum of sea ice occurs. This amplified autumn and winter warming contributes to a phenomenon called Arctic amplification (e.g., Serreze et al. 2009; Screen and Simmonds 2010b; Inoue and Hori 2011), which in turn alters the meridional temperature gradient between the equator and the pole, especially at the surface. This ice loss has also increased the moisture content of the Arctic atmosphere (Serreze et al. 2012), which may in part explain the observed increase in cyclone-associated precipitation during the recent warm period (Li et al. 2014). Several other studies document an increase in autumn/winter snowfall over the adjacent boreal land in recent years of anomalously low summer sea ice, particularly over Siberia (e.g., Ghatak et al. 2010, 2012; Cohen et al. 2012; Liu et al. 2012; Orsolini et al. 2012).

Nevertheless, how these atmospheric changes in response to sea ice loss manifest with regard to cyclone frequency and intensity within the Arctic remains unclear. Changes in cyclone tracks, frequency, and intensity reflect competing processes, such as changing temperature gradients between midlatitudes and the pole, and changes in specific humidity as the atmosphere warms. This has resulted in studies reaching different conclusions, with some studies suggesting a reduction in midlatitude cyclone frequency and intensity during winter (e.g., Gitelman et al. 1997; Geng and Sugi 2003), while others suggesting an increase in frequency and strength of winter cyclones (Bengtsson et al. 2006; Simmonds et al. 2008; Sorteberg and Walsh 2008; Simmonds and Keay 2009; Stroeve et al. 2011), depending on the time period evaluated and the metrics used to identify cyclones.

One consequence of sea ice loss and associated autumn warming that appears less uncertain is the potential for a poleward shift of storm tracks related to a northward shift in the region of greatest baroclinic instability (e.g., Hall et al. 1994; Carnell et al. 1996). Several studies report that a northward shift of storm tracks has already occurred, related to reduced winter sea ice in the Barents and Kara Seas, which may in turn be partly responsible for the warm Arctic–cold Eurasian continent pattern (e.g., Bengtsson et al. 2006; Inoue et al. 2012; Tang et al. 2013), although the role of sea ice loss in the cold continent pattern is disputed (Sun et al. 2016; Sorokina et al. 2016). Future projections for the end of this century in an anthropogenically warmed climate also suggest a northward shift will occur, yet the number of cyclones in the North Atlantic will actually decrease as a result of the midtroposphere warming faster than the ocean surface, thereby increasing vertical stability (Zahn and von Storch 2010).

In summary, while the position of the sea ice edge might be expected to impact cyclone development and their tracks, it remains uncertain if the recent northward progression of the summer ice edge has already influenced autumn and winter cyclone frequency and intensity. This study is motivated by these large uncertainties. We aim not only to document whether or not cyclone frequency and intensity have changed in response to sea ice retreat, but also to evaluate the physical mechanisms governing changes in cyclone activity and how that may change in a further warmed climate. It is hypothesized that reductions in summer SIE and expanding open water areas in September have already transformed moisture availability, regional baroclinicity, and atmospheric vertical stability in autumn. Building on previous work by Stroeve et al. (2011), this study uses data through 2014 and analyzes not only cyclone frequency and intensity, but also changes in extreme cyclones and the Eady growth rate, which can be strongly influenced by changes in the meridional temperature gradient. By comparing various cyclone metrics for low and high ice years, we hope to shed more light on the potential impacts of northward retreat of the ice edge on Arctic cyclone activity.

This paper is structured as follows: Section 2 briefly describes the data and methods used in this study, and how summer sea ice loss impacts the atmosphere is presented in section 3. Sections 4, 5, 6, and 7 report changes in baroclinic instability, vertical temperature difference, cyclone activity, and extreme cyclone activity, respectively, with respect to sea ice loss. Section 8 summarizes the results and presents discussion.

2. Methodology

There is no universal agreement on how exactly to define what constitutes an extratropical cyclone and where it is located. Despite their inherent complexity, many researchers have explored objective cyclone identification and tracking methods over the last two decades (Neu et al. 2013). Among currently available schemes, the Serreze et al. (1997) cyclone detection method has been used in numerous studies to monitor extratropical cyclones, mainly in the Northern Hemisphere (e.g., McCabe et al. 2001; Serreze and Etringer 2003; Wang et al. 2006; Finnis et al. 2007; Tsukernik et al. 2007;
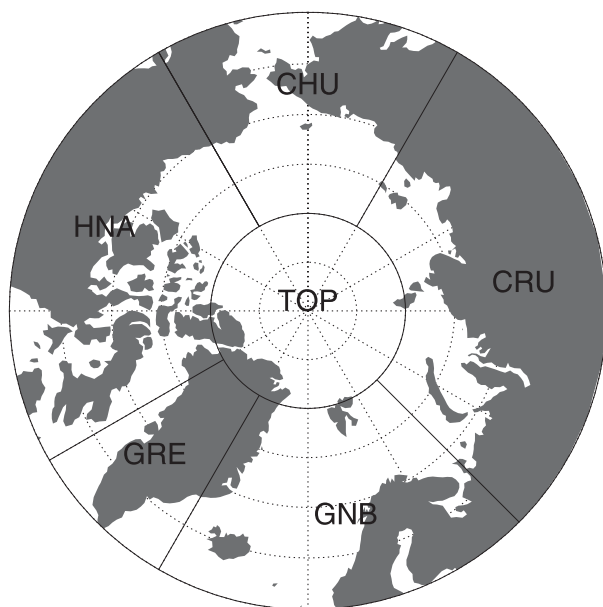
FIG. 1. The entire Arctic (ARC) north of 60°N includes the high-latitude North America (HNA), the Chukchi and East Siberian Seas (CHU), central Russia (CRU), the Greenland, Norwegian, and Barents Seas (GNB), Greenland (GRE), and all areas north of 80°N (TOP).

Serreze and Barrett 2008; Stroeve et al. 2011). We also rely on the Serreze et al. (1997) method to identify and track cyclones, where cyclones are tracked based on a series of search patterns to define occurrences when sea level pressure (SLP) is at least 1 hPa lower than adjacent grid points (described in more detail below).

We additionally evaluate vertical temperature difference, baroclinic instability, cyclone intensity, and frequency of extreme cyclones. The Eady growth rate (Hoskins and Valdes 1990) provides a measure of baroclinicity and is determined by changes in static stability and vertical wind shear. Cyclone intensity is given by the cyclone central pressure and the local Laplacian. Details on each cyclone metric evaluated are provided in sections 2b through 2d below. As in Stroeve et al. (2011) we summarize results for the entire Arctic and also for different regions as depicted in Fig. 1.

a. Data

Among currently available reanalysis products, we mainly rely on the National Centers for Environmental Prediction (NCEP)–National Center for Atmospheric Research (NCAR) reanalysis (Kalnay et al. 1996), in part to be consistent with earlier work by Serreze et al. (1997), and also to extend the Northern Hemisphere cyclone locations and characteristics dataset originally developed by Serreze et al. (2009) and distributed by the National Snow and Ice Data Center

(NSIDC; https://nsidc.org/data/docs/daac/nsidc0423_cyclone/) through 2008. A drawback is that it has lower horizontal and vertical resolution than more modern reanalysis datasets. Accordingly, two more modern products, the ECMWF interim reanalysis (ERA-Interim; Dee et al. 2011) and Modern-Era Retrospective Analysis for Research and Applications (MERRA; Rienecker et al. 2011) are utilized to verify the robustness of the results.

The target period of this study, from 1979 to 2014, is inherently determined by the time period of available sea ice data observed by satellites. Sea ice observations by multichannel passive microwave sensors did not become available until October 1978. While some prior satellite observations are available, these are not consistent in time or spatial coverage. We use observations of sea ice concentration from the NASA Team Scanning Multichannel Microwave Radiometer and Special Sensor Microwave Imager dataset (Cavalieri et al. 1999) obtained from NSIDC. SIE is defined as the total ice area with at least 15% sea ice concentration.

To isolate potential links between reduced summer sea ice and changes in cyclone activity during the following months, we focus our analysis on relationships between mean September SIE (the SIE at the end of the summer melt season) and indices of cyclone activity from September to November for several different time periods. These are defined by sorting the September SIE north of 60°N in ascending order, pentad, decade, and 18-yr (half of the entire record) duration periods, for which the lowest and highest SIE are selected for each time period. Extreme high and low sea ice years are additionally determined by selecting years with values greater than ±1.0 standard deviation (SD) from the standardized time series, (i.e., the SIE time series is depicted as areal unit variation standardized to have a unit SD and zero mean value). The linear trend is computed by minimizing the chi-square error statistic. Figure 2 shows the standardized September and December SIE time series and the extreme years with box symbols. The December SIE trend is used for extreme cyclone analysis discussed later. Table 1 lists the September and December low and high ice years corresponding to each of the four time periods evaluated.

b. Eady growth rate

The theory of baroclinic instability pioneered by Charney (1947) and Eady (1949) provides a physical explanation of cyclogenesis (Descamps et al. 2007). The maximum Eady growth rate is commonly used to measure development of atmospheric wave disturbances and is used as a measure of the potential for cyclones to develop and strengthen (Hoskins and Valdes 1990; Paciorek et al. 2002; Lim and Simmonds 2007; Serreze and Barrett 2008). Here we determine the Eady growth rate σ at each grid
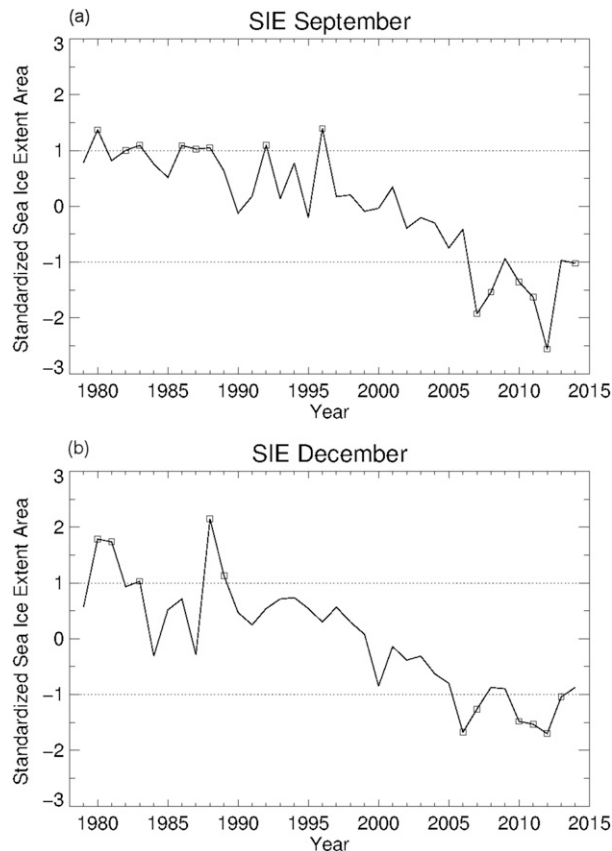
FIG. 2. Standardized SIE time series from 1979 to 2014 for (a) September and (b) December. The extreme ice years are listed in Table 1. Box symbols correspond to those extreme years.

point for each day at 500 hPa following Paciorek et al. (2002) and Vallis (2006):

$$\sigma \equiv 0.31 \frac{f}{N} \left| \frac{\partial \mathbf{v}}{\partial z} \right|, \tag{1}$$

where f is the Coriolis parameter, N is the Brunt–Väisälä frequency (Rogers 1978; Lee and Mak 1994), z is the

vertical distance, and $\mathbf{v}$ is the horizontal wind vector. The vertical wind shear ($\partial \mathbf{v}/\partial z$) is related to the horizontal temperature gradient via the thermal wind equation (Wallace and Hobbs 2006). The Brunt–Väisälä frequency, which is a measure of atmospheric static stability, is given by

$$N = \left(\frac{g}{\theta} \frac{d\theta}{dz} \right)^{1/2}, \tag{2}$$

where g is the acceleration due to gravity and θ is the potential temperature. One can see that the Eady growth rate depends on *both* the static stability and horizontal temperature gradients in the atmosphere. Following Simmonds and Lim (2009), the potential temperatures at 300, 500, and 700 hPa are used to estimate N and $\partial \mathbf{v}/\partial z$. The zonal and meridional winds, air temperature, and geopotential height fields directly from NCEP–NCAR reanalysis and the potential temperature calculated from the reanalysis temperature and pressure are utilized for the derivation. Simmonds and Lim (2009) further showed that the Eady growth rate derived from the time-mean fields is not entirely suitable and instead recommend computing σ at all relevant synoptic time scales before averaging. Accordingly, daily products are utilized to estimate the Eady growth rate.

c. Cyclone detection

The Serreze et al. (1997) cyclone tracking algorithm uses a series of search patterns to detect cyclones: the cyclone center is assumed to be defined when the SLP is at least 1 hPa lower than the adjacent grid points. The algorithm employs a nearest-neighbor analysis of the positions of cyclones from temporally successive SLP fields. Assuming two thresholds, a maximum search distance and an allowable pressure difference, the tracking algorithm examines if a target cyclone has moved in sequential time steps. To track center jumps, those limiting values are set at 800 km and 20 hPa, respectively.

TABLE 1. September and December SIE low and high periods from 1979 to 2014. Refer to section 2a data and Fig. 2 for the methodology of determining the low and high ice years.

Period	Sep low years	Dec low years	Sep high years	Dec high years
Pentad	2007, 2008, 2010, 2011, 2012	2006, 2007, 2010, 2011, 2012	1980, 1983, 1986, 1992, 1996	1980, 1981, 1983, 1988, 1989
Decade	2005, 2006, 2007, 2008, 2009, 2010, 2011, 2012, 2013, 2014	2000, 2006, 2007, 2008, 2009, 2010, 2011, 2012, 2013, 2014	1979, 1980, 1981, 1982, 1983, 1986, 1987, 1988, 1992, 1996	1979, 1980, 1981, 1982, 1983, 1986, 1988, 1989, 1993, 1994
18 yr	1990, 1993, 1995, 1999, 2000, 2002, 2003, 2004, 2005, 2006, 2007, 2008, 2009, 2010, 2011, 2012, 2013, 2014	1984, 1987, 1999, 2000, 2001, 2002, 2003, 2004, 2005, 2006, 2007, 2008, 2009, 2010, 2011, 2012, 2013, 2014	1979, 1980, 1981, 1982, 1983, 1984, 1985, 1986, 1987, 1988, 1989, 1991, 1992, 1994, 1996, 1997, 1998, 2001	1979, 1980, 1981, 1982, 1983, 1985, 1986, 1988, 1989, 1990, 1991, 1992, 1993, 1994, 1995, 1996, 1997, 1998
≥ 1.0 |SD|	2007, 2008, 2010, 2011, 2012, 2014	2006, 2007, 2010, 2011, 2013	1980, 1982, 1983, 1986, 1987, 1988, 1992, 1996	1980, 1981, 1983, 1988, 1999

To select robust cyclone systems in the Arctic (60°–90°N), only cyclones satisfying the following three criteria are considered: 1) cyclones must last more than 24 h, 2) cyclones must not be stationary, and 3) a cyclone must deepen at least 2 hPa during its life cycle (Serreze and Barrett 2008). Regions with surface elevations higher than 2000 m are discarded since the tracking algorithm tends to detect spurious systems over mountainous terrain where there is larger uncertainty in the utilized SLP fields. For example, Rudeva et al. (2014) showed that the Serreze tracking algorithm tracked the highest number of cyclone tracks in a selected region in central Asia among 13 schemes evaluated. By applying topographic filtering, the number of tracked cyclones becomes close to the ones detected using other schemes. Similar terrain filtering is widely used as a part of cyclone tracking algorithms (Neu et al. 2013).

The intensity of an individual cyclone can be quantified in terms of the cyclone central pressure and local Laplacian at each cyclone center. However, cyclone central pressure only gives a rough indication of cyclone strength since airflow near the surface is largely affected by pressure difference between cyclone center and SLP field on the periphery. Thus, it is necessary to consider an ambient pressure field when we discuss central pressure in the context of cyclone intensity. On the other hand, the Laplacian is proportional to the geostrophic relative vorticity and directly indicates the corresponding cyclone intensity.

We perform a further consistency check using ERA-Interim and MERRA. While the horizontal resolutions of ERA-Interim and MERRA are 0.75° × 0.75° and ⅔° longitude by 0.5° latitude, respectively, the SLP field is regridded into 100 km × 100 km spatial resolution for the tracking algorithm application. Since the spatial resolution is still finer than the NCEP–NCAR reanalysis, a multicenter cyclone detection procedure is applied in the tracking: when there are two cyclone centers that are clearly part of the same system, the system will only be counted as one cyclone. Topographic filtering is not applied since ERA-Interim and MERRA use more advanced assimilation techniques.

d. Extreme cyclones

In this study, extreme cyclones are determined from daily SLP fields following previous studies (Chang et al. 2012; Vavrus 2013). The climatological annual average SLP at each grid point is first determined from 1981 to 2010. When the SLP for a specific grid cell at a specific time is at least 40 hPa lower than the climatological value at the same grid point, it is assumed that an extreme cyclone occurred in that location. There is an advantage of using "relative" central pressure to study

cyclones (Simmonds et al. 2003). Strong local meridional pressure gradients over the subarctic region and the locations vary by season (Serreze and Barry 2014) so that when a midlatitude cyclone migrates poleward, the central pressure may decrease even if it is not intensifying. Also, how cyclones are defined—as minima in the total SLP or as minima in SLP perturbations after a large-scale, low-frequency background flow has been removed—has an impact on projection of change in the frequency of strong cyclones over the Pacific under global warming (Chang 2014). While this approach does not show cyclone tracks, it can identify instances of extremely strong cyclones without needing to consider anomalous cyclonic or anticyclonic systems.

Figure 3a shows the climatological mean monthly occurrence of extreme cyclones based on NCEP–NCAR reanalysis. The southern boundary of the Arctic domain is extended from 60° to 50°N since the latitude of the climatological center for the Aleutian low exists near 50°N. Seasonal variation of the annual cycle is apparent: while extreme cyclones hardly occur in summer, the number of extreme cyclones increases during autumn and winter, reaching a maximum in January. This seasonal cycle agrees with previous studies (Zhang et al. 2004; Vavrus 2013). Spatially, the highest frequency in annual extreme cyclones occurs over Iceland and in the vicinity of the Icelandic low (Fig. 3b). The surrounding area where the average count is above 1.5 extreme cyclones per year corresponds to the North Atlantic cyclone track. Another area of high frequency of extreme cyclones lies in the Bering Sea, corresponding to the winter Aleutian low. The spatial pattern is similar to that obtained using MERRA reanalysis (Vavrus 2013), while the derived frequencies by MERRA are greater than those of NCEP–NCAR.

3. Atmospheric impacts of summer sea ice loss

Since cyclone intensification and dissipation is sensitive, among other influences, to heat exchange processes at the surface (e.g., Kuo et al. 1991), the presence or absence of sea ice might be expected to play an important role in this heat exchange, leading to changes in cyclone activity.

Figure 4 shows September sea ice area differences together with differences in autumn (SON) ERA-Interim sensible and latent heat fluxes, 925-hPa air temperatures, and precipitable water between low and high ice years, determined by subtracting the high ice period from the low ice period. By conducting paired *t* tests, these differences are found to be statistically significant except for mean sensible heat flux differences corresponding to the ±1.0 SD period. Extensive sea ice
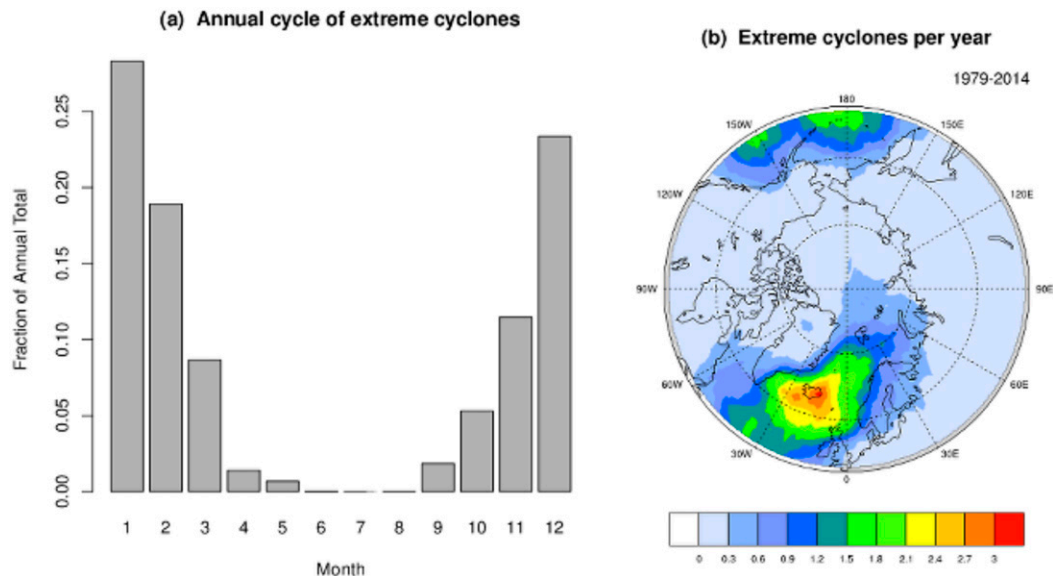
FIG. 3. (a) Annual cycle of extreme cyclones determined from daily NCEP–NCAR SLP field of 1981–2010.
(b) Annual mean count of extreme cyclones from 1979 to 2014.

loss is observed within the Beaufort, Chukchi, East Si-
berian, and Laptev Seas for the four composite time
periods, with the largest reductions observed for the
pentad and the ±1.0 SD composites. Reductions are
considerably less in the East Greenland Sea, Baffin Bay,
and Barents Sea.

The local autumn atmospheric response of ice loss
manifests as negative anomalies in the turbulent heat
fluxes. Local minima of the sensible and latent heat flux
anomalies coincide with regions of large summer ice loss
(e.g., the Beaufort, Chukchi, Laptev, and Kara Seas as well
as in the northern Barents Sea). On the other hand, pos-
itive differences are dominant in the Bering, Barents, East
Greenland, and Labrador Seas. Little difference is ob-
served over the middle of the Arctic Ocean where sea ice
coverage has been stable. It is suspected that decreases in
turbulent heat fluxes during low ice years reflect a smaller
vertical temperature gradient between the sea surface and
overlying air in close proximity to each other, which is also
influenced by advection of warm air. Over the open ocean
farther south, the sensible and latent heat fluxes increase
along with increased sea surface temperatures (SSTs),
resulting in positive differences. Negative differences in
Denmark Strait can be related to anomalous cooling of the
Irminger Sea (e.g., de Jong and de Steur 2016).

Increased heat loss from the ocean to the atmosphere
in autumn helps to explain positive anomalies in air
temperature throughout the Arctic at 925 hPa (Fig. 4,
fourth row). Particularly large anomalies extend from
the East Siberian Sea shore to the west of Severnaya
Zemlya via north of the Laptev Sea. The largest positive

anomalies occur during the pentad and ±1.0 SD com-
posite periods, consistent with the time periods with the
largest ice loss. Woods and Caballero (2016) studied
poleward intrusions of moist air across 70°N from Oc-
tober to January and showed that the vertical structure
of the warming associated with moist intrusion is bottom
amplified: a trend toward a weakening of the climato-
logical temperature inversion. However, it is still un-
known how much the moisture flux into the Arctic
affects the SON 925-hPa temperature field since the
frequency of intrusion events in October and November
does not show statistically significant increment.

The last row of Fig. 4 shows corresponding anomalies
in precipitable water. The areas of predominantly posi-
tive anomalies partially correspond to areas of sea ice
loss and 925-hPa temperature anomalies (i.e., near the
East Siberian Sea and Severnaya Zemlya). This is ex-
pected since precipitable water is largely dependent on
the moisture content in the lower troposphere, and a
warmer atmosphere is able to hold more moisture.
Furthermore, positive anomalies of precipitable water
appear over the North Atlantic and the Barents and
Labrador Seas during the pentad and the ±1.0 SD
composites. More frequent moist intrusions into the
central Arctic basin can be expected during low ice years
(Woods and Caballero 2016). Consequently, the in-
creases in precipitable water reflect increased moisture
and temperature as well as a contribution from bottom-
amplified warming. A transition from a "cold clear" to a
"warm opaque" state can in turn yield increased
downwelling longwave radiation (Stramler et al. 2011).

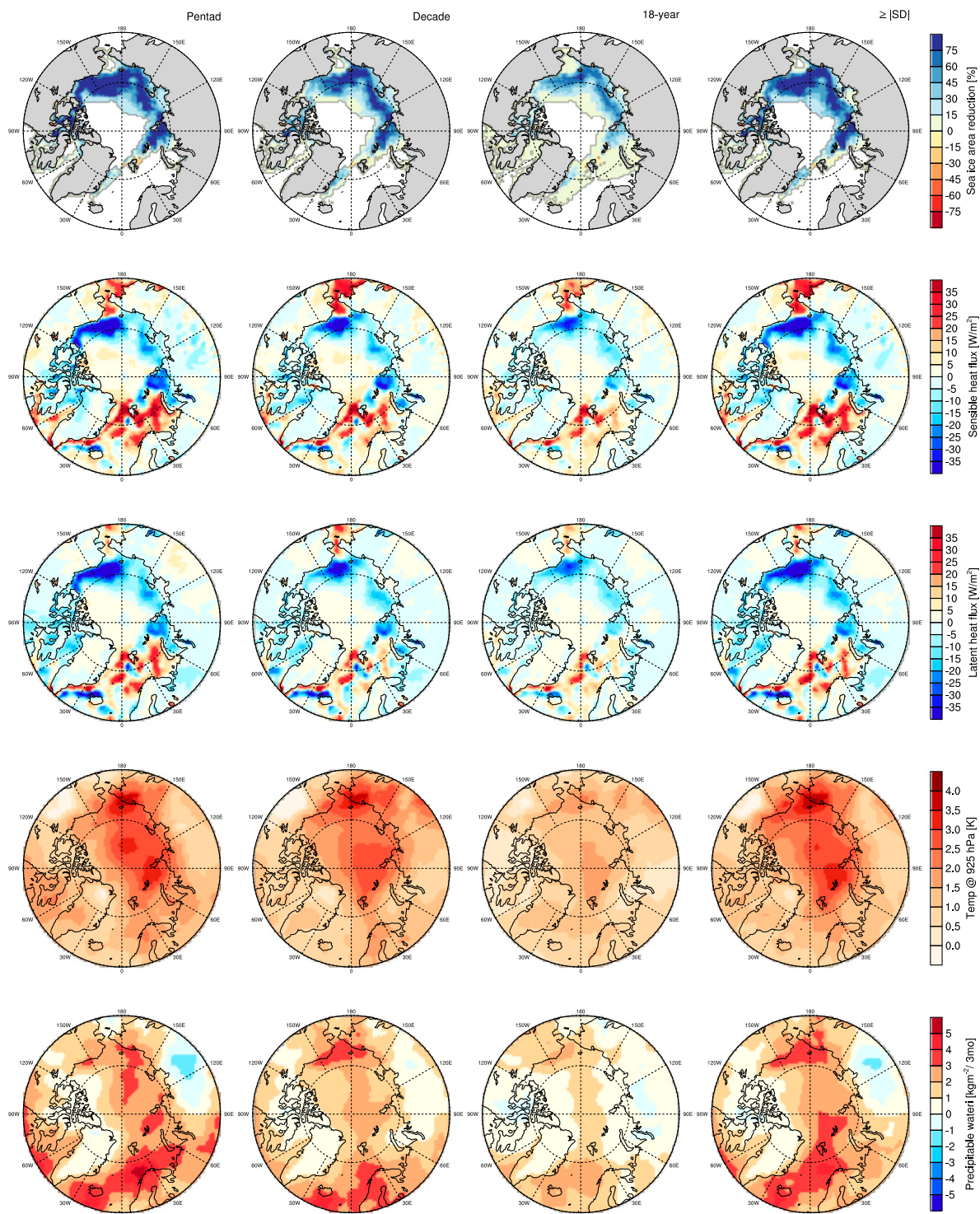# Difference in SON: "Low ice years" minus "High ice years"

FIG. 4. (from top to bottom) Composite September sea ice area change ratio from the high ice years to low ice periods; mean sensible heat flux; mean latent heat flux; mean 925-hPa air temperature; and mean precipitable water. Each column period can be referred to Table 1. ERA-Interim is utilized except for the first row.

While these physical hypotheses are based on interpreting the composite results, composite patterns may be misleading (Boschat et al. 2016). Their analysis initially suggested that SST dipole conditions may form a *necessary* condition for summer heat waves. However, sensitivity tests indicated that the vast majority of days when the dipole SST pattern appeared were not associated with heat waves (i.e., the SST dipole pattern was not a *sufficient* condition). Thus, more rigorous evaluation is required to confirm exactly how sea ice reduction affects the heat exchange processes. However, we aim to only broadly explore the association between Arctic sea ice loss and changes in different environmental variables that can potentially impact cyclone development.

4. Changes in vertical temperature difference

Jaiser et al. (2012) documented that stronger heat release to the atmosphere, such as observed above, reduces the atmospheric vertical static stability when sea ice concentration is low, leading to an earlier onset of baroclinic instability. Zahn and von Storch (2010) utilized a simplified measure of vertical stability, the temperature difference between sea surface and at 500-hPa model levels, and showed that the increased vertical temperature gradient contributes to weakened polar lows: polar lows are intense maritime mesoscale cyclones forming at high latitudes during cold air outbreaks (Rasmussen and Turner 2003). Since this measure is useful to detect unstable conditions related to polar low development, it is utilized for operational forecasting in Norway (e.g., Noer and Ovhed 2003; Woollings et al. 2012). Given that polar lows cannot always be detected by our cyclone tracking algorithm because of the coarse grid spacing of the reanalysis data fields, this measure is helpful not only for estimating favorable conditions for polar lows to form, but also for the potential for synoptic-scale cyclogenesis in the Arctic.

Figure 5 shows the mean values of the temperature difference between 500 and 925 hPa within the Arctic and six regions as shown in Fig. 1. Mean values are computed for the ±1.0 SD low and high sea ice years. The vertical temperature differences in each region during low ice years is generally larger, suggesting more favorable conditions for cyclogenesis during low sea ice years. Thus, the position of the ice edge appears to influence vertical stability, such that small-scale disturbances in low-level air flows formed during low years are more likely to develop into cyclones over most of the Arctic. While the results are generally consistent between the different reanalysis, the NCEP–NCAR

reanalysis shows considerably smaller temperature gradients over GRE that are likely an artifact of the coarser spatial resolution and small sample size of the GRE region (all regions are defined in Fig. 1).

5. Changes in baroclinic instability

Eady growth rate measures the baroclinic instability around the midtroposphere level. This altitude is effective for depicting the synoptic-scale potential for storminess. Regional time series of all grid cells with an Eady growth rate exceeding a threshold of $\sigma > 1.5 \, \text{day}^{-1}$ in autumn from NCEP–NCAR reanalysis are shown in Fig. 6. The average Eady growth rate over the domain during the study period is $0.52 \, \text{day}^{-1}$. Since the threshold value is approximately 3 times the average, it is only exceeded when strong cyclones occur, such as the Great Arctic Cyclone (Simmonds and Rudeva 2012; Parkinson and Comiso 2013; Zhang et al. 2013; Yamazaki et al. 2015). The annually averaged number of cyclones within the TOP, GRE, HNA, CHU, CRU, and GNB regions (see Fig. 1) during the study period are 45.3, 130.8, 224.6, 58.0, 69.6, and 199.3, respectively, indicating cyclones are more likely to occur in the GNB and HNA regions during autumn, where baroclinic instability can contribute to intensification and persistence of cyclones. However, while positive trends in Eady growth rate are seen in several regions of the Arctic (e.g., GRE, HNA, CRU, and GNB regions), only the GRE region shows statistically significant increases in baroclinic instability ($p \leq 0.05$).

To examine the influence of the reanalysis dataset, Fig. 7 shows mean counts of grid cells where $\sigma > 1.5 \, \text{day}^{-1}$ in autumn from three reanalyses during the ±1.0 SD high and low ice years. Mean counts are normalized by the total number of grid points over the domain since each reanalysis has different spatial resolution. NCEP–NCAR results in larger frequency of occurrence during low ice years in all regions, whereas MERRA and ERA-Interim give mixed results. The same analysis was performed on October and November SIE ±1.0 SD composites (not shown). Only within the GRE region do we find consistency among the reanalysis products that there is a tendency for increased autumn baroclinicity during low sea ice years. In other words, baroclinic instability increases over Greenland following anomalously low sea ice conditions in autumn.

6. Changes in cyclone activity

a. Interannual variability and trend analysis

Given the above indications of a moist climate, the potential for increased baroclinicity around Greenland,
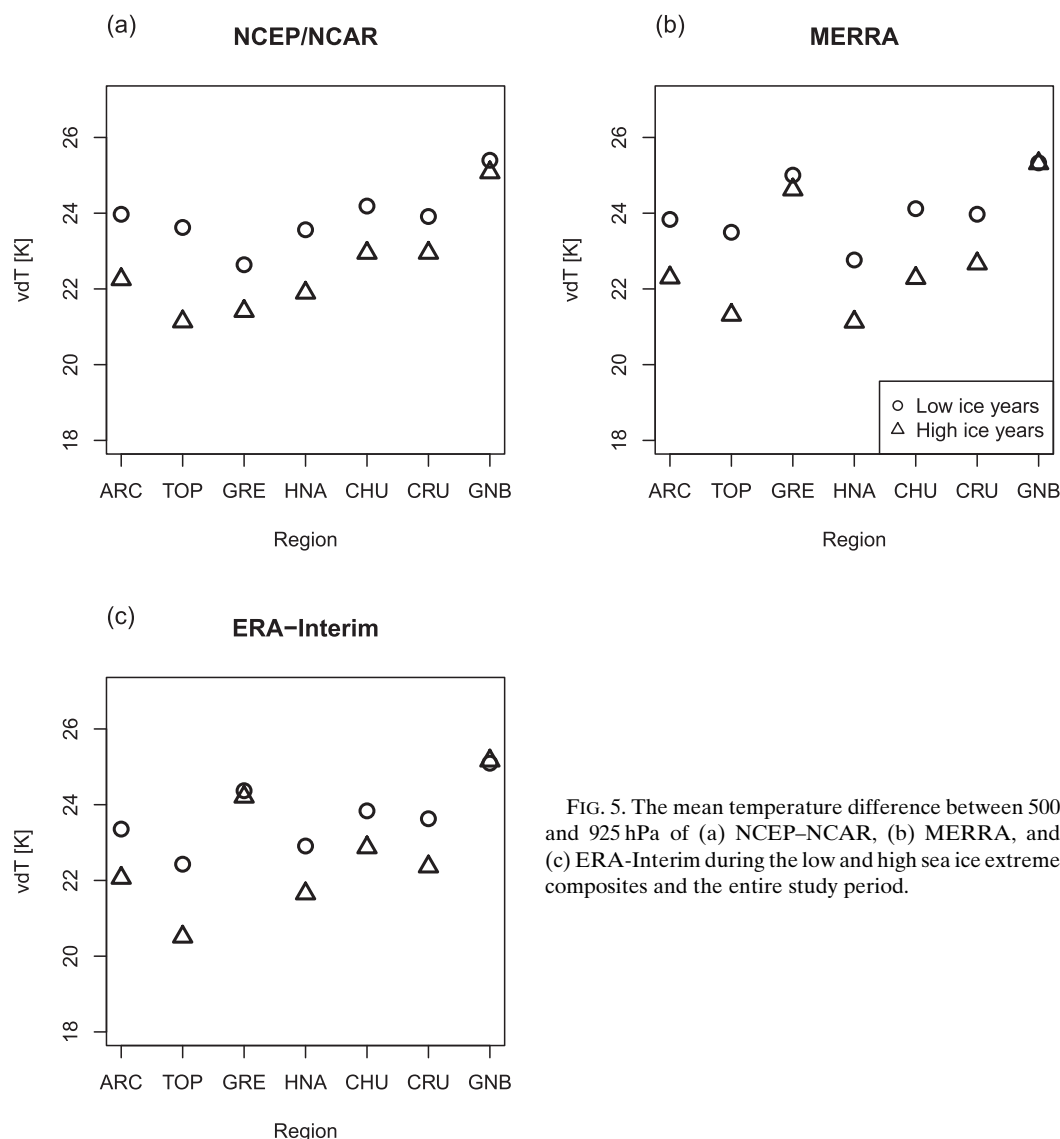
Vertical Temperature Difference

FIG. 5. The mean temperature difference between 500 and 925 hPa of (a) NCEP–NCAR, (b) MERRA, and (c) ERA-Interim during the low and high sea ice extreme composites and the entire study period.

and larger vertical temperature difference during low sea ice years, we now examine whether these changes have actually influenced cyclone activity in the Arctic. Cyclone counts show large seasonal and interannual variability (Fig. 8 and Table 2). Cyclone frequency peaks in summer, in agreement with Serreze and Barrett (2008) and Simmonds et al. (2008). Spring and autumn generally show similar number of cyclones, but with slightly more frequent cyclones in autumn (85 vs 79). While monthly SIE shows negative trends in all months (not shown), positive trends are only seen in autumn (+0.6 cyclones per decade), yet they are not statistically significant. The only season with a statistically significant trend is summer, decreasing at a rate of 3.3 cyclones per decade.

b. Cyclone deepening rates

Figure 9 shows averaged maximum cyclone deepening rates in autumn for three time periods (a) 1979–2014, (b) +1.0 SD high ice years, and (c) −1.0 SD low ice years from NCEP–NCAR reanalysis. The cyclone deepening rate is defined as the change in 6-hourly cyclone center pressure. The location of maximum cyclone deepening is a good indicator of where the strongest development occurs (Serreze and Barrett 2008). The average maximum cyclone deepening rate
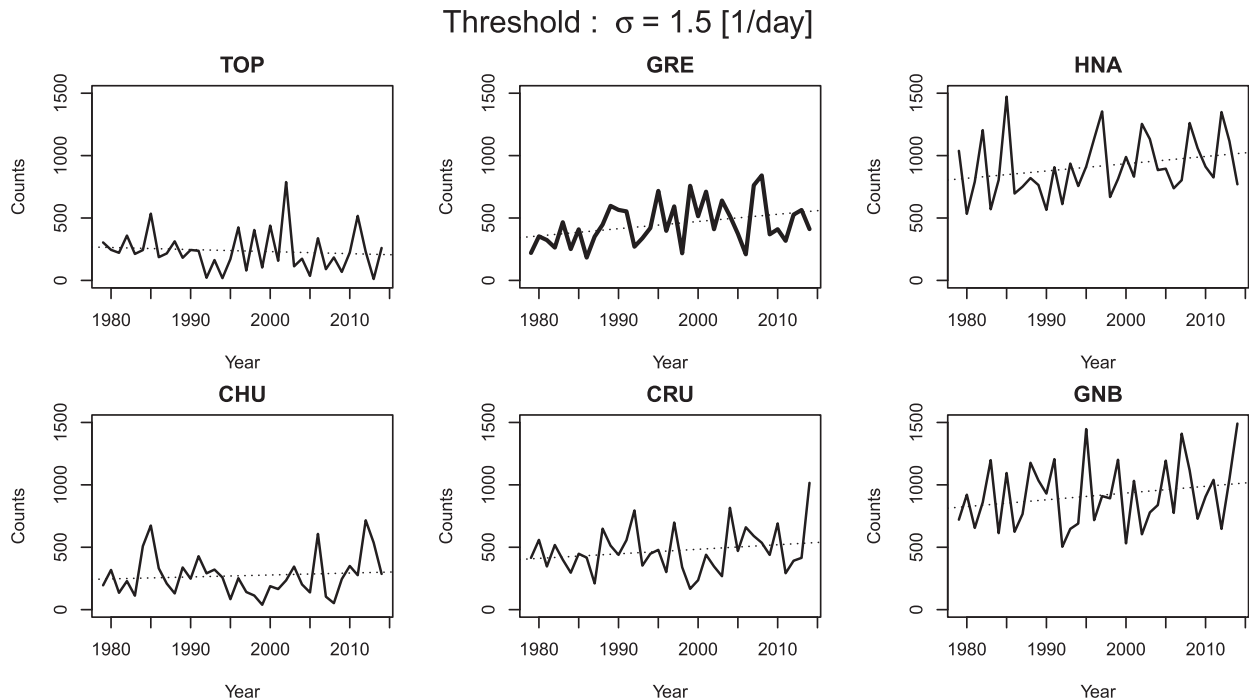
FIG. 6. Regional trends of grid cell numbers exceeding the threshold $\sigma = 1.5$ day^{-1}, which is based on NCEP–NCAR reanalysis. The GRE region demonstrates a statistically significant trend. The dotted lines are linearized trends.

is defined as the summation of the maximum deepening rates divided by the number of the maximum deepening events. Locally, deepening rates are largest from Denmark Strait to the Greenland Sea and there is some indication that maximum deepening rates are increasing poleward in the Barents Sea during low ice years. However, caution is needed as these results are influenced by sample size differences: while the entire study period has samples over 36 years, those of high and low ice periods are collected from periods of 8- and 6-yr duration, respectively. The numbers of detected cyclones at a grid point during low ice periods are smaller than those of the entire study period. Since depicted cyclone deepening rates are the sample mean of maximum cyclone deepening rates, their confidence intervals are not consistent. Assuming a 95% confidence level, confidence intervals for the entire time series and high ice and low ice periods are 0.4178–0.4281, 0.4307–0.4458, and 0.4220–0.4387, respectively. Thus, the lengths of the confidence intervals for the high and low ice years are larger than that for the entire study period.

Corresponding frequency distributions of maximum deepening rates show that the most frequent maximum deepening rate is between 0.3 and 0.4 hPa hour^{-1} regardless of compositing (Fig. 10). Mean values of the maximum cyclone deepening rates for 1979–2014 and for the high and low ice years are 0.38, 0.38, and

0.37 hPa hour^{-1}, respectively, suggesting no specific tendency in cyclone deepening rates between high and low ice years.

c. Spatial pattern of cyclone activity

Cyclone activity with respect to SIE variation is analyzed in an analogous way to the surface energy budget analysis. Figure 11 shows low minus high ice year differences in SON sea ice area, mean cyclone counts, cyclone center mean SLPs, and the local Laplacian derived from NCEP–NCAR reanalysis.

Small and unevenly shaped positive and negative anomalies in cyclone frequency are found for all different composites throughout the Arctic (Fig. 11, second row). Weak positive anomalies occur in Baffin Bay, south of Denmark Strait, north of Norway, the vicinity of Severnaya Zemlya, and the Bering Strait. Considering patterns of the pentad and the ±1.0 SD composites, positive anomalies north of Norway might correspond to a marked increase in autumn cyclone activity within the GNB region previously reported by Stroeve et al. (2011); however, the spatial pattern is more limited and less coherent. In particular, positive anomalies are interspersed with negative anomalies, and it is difficult to find a specific pattern of anomalies along with the area where extreme cyclones frequently occur. In addition, differences are only statistically significant ($p \leq 0.01$) for the decade and
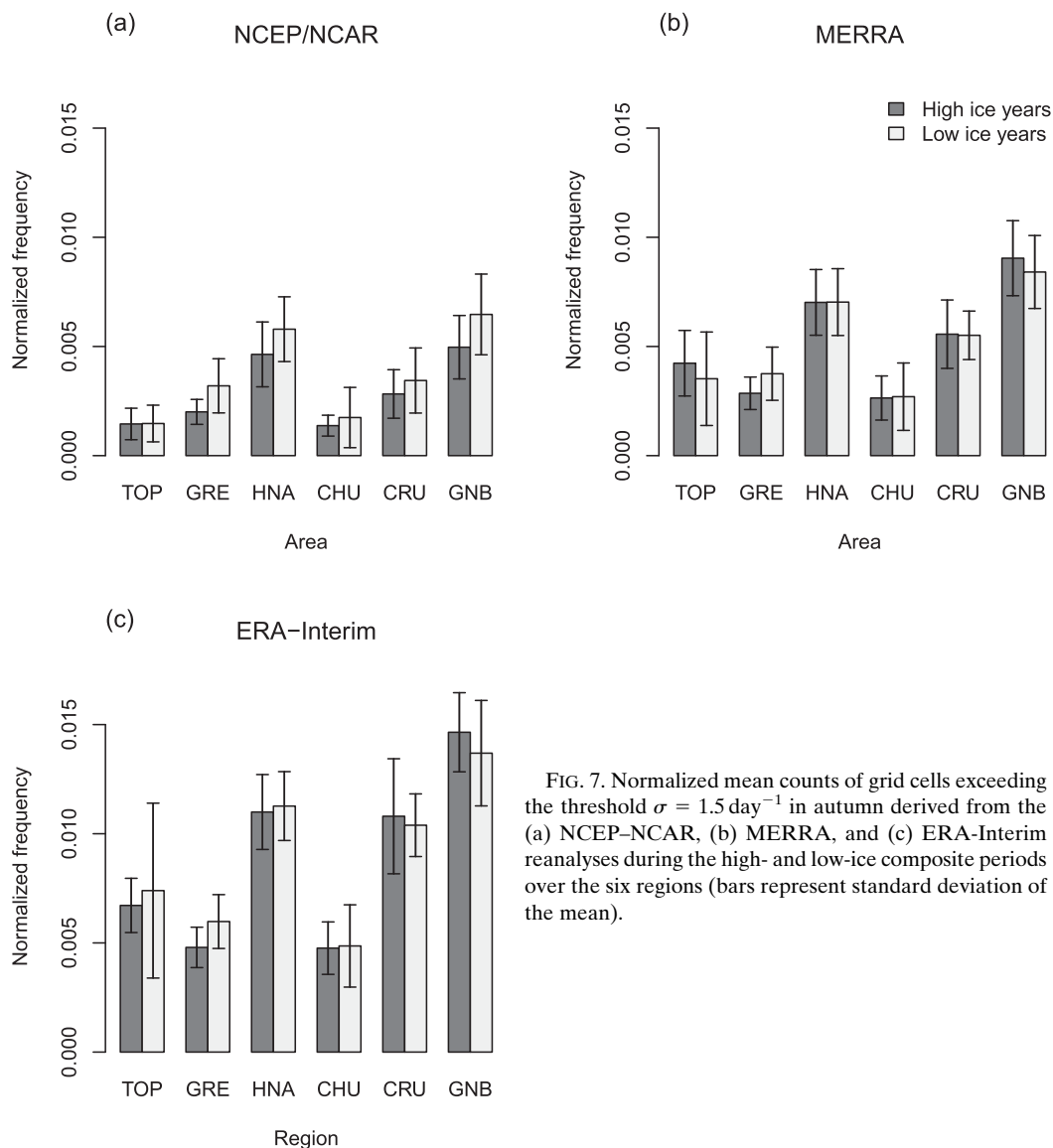
Mean counts exceeding threshold σ =1.5

(a)   NCEP/NCAR

(b)   MERRA

(c)   ERA−Interim

FIG. 7. Normalized mean counts of grid cells exceeding the threshold $\sigma = 1.5\,\text{day}^{-1}$ in autumn derived from the (a) NCEP–NCAR, (b) MERRA, and (c) ERA-Interim reanalyses during the high- and low-ice composite periods over the six regions (bars represent standard deviation of the mean).

±1.0 SD years, but not for the pentad and the 18-yr composite.

Regions with large summer ice losses generally show little change in cyclone activity except for some small increases in frequency in the Laptev, Kara, and Barents Seas, but again, these regions are interspersed with declines in cyclone activity as well, making it difficult to ascribe these changes directly to sea ice loss. Interestingly, no real change in cyclone activity is found over North America. The correlation coefficients between mean changes in sea ice area and mean changes in cyclone frequency for the pentad, decade, 18-yr, and ±1.0 SD periods are 0.04, 0.13, 0.07, and 0.07,

respectively, which are not statistically significant. Thus, the results do not suggest that cyclone frequency has changed in response to sea ice loss.

Turning our attention toward cyclone intensity, we find that all Laplacian differences and the pentad and decade composites of SLPs are statistically significant ($p \leq 0.01$), while the 18-yr and ±1.0 SD composites of SLPs are not (Fig. 11, rows 3 and 4). Changes in intensity might be expected to occur when the sea ice area represents a major change (i.e., because of averaging, the longer the duration becomes, the less the corresponding anomalies show). Thus, we can expect that spatial patterns are better defined for the pentad and
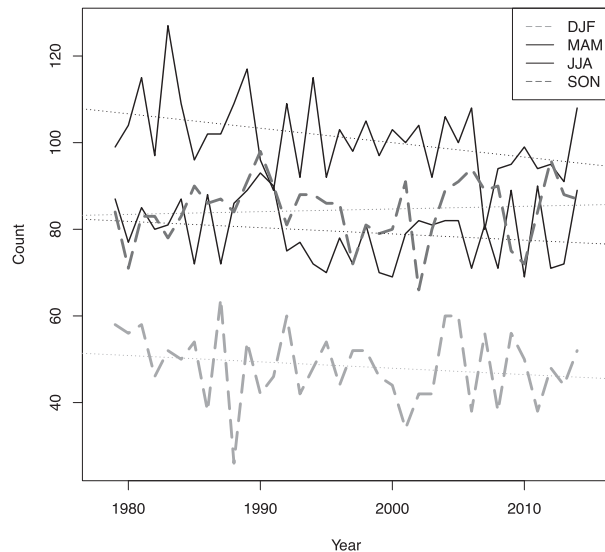
FIG. 8. Time series of seasonal cyclone counts derived from NCEP–NCAR reanalysis over the Arctic. The linearized trends are illustrated by dotted lines.

TABLE 2. Summary of seasonal cyclone counts variations.

Season	Mean	Standard deviation	Trend (count per year)	P value
Winter (DJF)	48.4	8.5	−0.15	0.29
Spring (MAM)	79.4	7.4	−0.14	0.23
Summer (JJA)	101.2	9.1	−0.33	0.020
Autumn (SON)	84.5	7.2	0.06	0.60

±1.0 SD composites than for the decade and 18-yr composites. Positive SLP differences are found in the Chukchi Sea, near the pole, and over large parts of Eurasia, combined with negative differences over Baffin Bay, the North Atlantic, and north of the Barents and Kara Seas during the pentad and ±1.0 SD composites. Positive (negative) SLP differences demonstrate that SLP during low ice years is higher (lower) than during high ice years, which indicates that cyclone intensity is weakened (intensified) with respect to sea ice loss. On the other hand, positive Laplacian differences indicate strengthened intensity since the local Laplacian is proportional to the geostrophic relative vorticity. Together the cyclone SLP and Laplacian suggest that while cyclone frequency may not be changing in the GNB and northern Barents and Kara Seas, cyclones are becoming more intense. However, correlation coefficients between area-weighted mean September SIE and the area-weighted mean local Laplacian in autumn are not statistically significant in any of the six regions. Since the GNB region tends to be ice free in summers, intensification of cyclones may be more related to observed increases in precipitable water.

Finally, to test the robustness of the results, corresponding differences in composite mean cyclone frequency, cyclone center mean SLPs, and the local Laplacian in SON derived from ERA-Interim and MERRA are shown in Fig. 12. Results remain noisy, and differences between low and high ice years are found to not be statistically significant by conducting

paired t tests. Nevertheless, features seen in the NCEP–NCAR reanalysis are also seen in MERRA and ERA-Interim, such as positive differences in mean cyclone frequency in northern Baffin Bay, the vicinity of the Icelandic low region, off the Kola Peninsula, Norway, and near the pole, together with weak negative differences in the Beaufort Sea. Less agreement is seen around Siberia. MERRA further indicates negative differences from Ellesmere Island to northwestern Greenland, which may be spurious a signal. Further study is required to assess if this is a limitation of the tracking algorithm, which is optimized for NCEP–NCAR reanalysis, or if it is a characteristic of the MERRA SLP field.

Spatial difference patterns in central SLPs and local Laplacian also generally agree among the reanalysis, the exception being that the magnitude of changes between the two composites is less in MERRA and ERA-Interim (Fig. 11, row 4; Fig. 12, rows 5 and 6). It is hypothesized that the local Laplacian derived from NCEP–NCAR has larger discretization error due to the coarse spatial resolution, resulting in larger differences between the high and low ice years. Overall, comparison among the three reanalysis products suggests that cyclone intensity is likely to be weakening in the Bering and Chukchi Seas, but the increase in cyclone intensity in the northern Barents and Kara Seas as well as in the North Atlantic is not robust.

7. Changes in extreme cyclone activity

Finally, we turn our attention to changes in extreme cyclone activity. Extreme cyclones mostly occur in winter (DJF) (Fig. 3a). Accordingly, high and low ice years are composited based on the December SIE (Table 2). Time series of DJF extreme cyclone counts over the GNB region and the entire Arctic (60°–90°N) show decreasing trends on the order of −2.84 and −6.71 counts per year, respectively, yet are not statistically significant (Fig. 13). Variability in extreme cyclones appears closely linked with the winter Arctic Oscillation (AO) (Thompson and Wallace 1998) (Fig. 13b). Correlation coefficients between the DJF AO index and extreme cyclone counts in the GNB region and
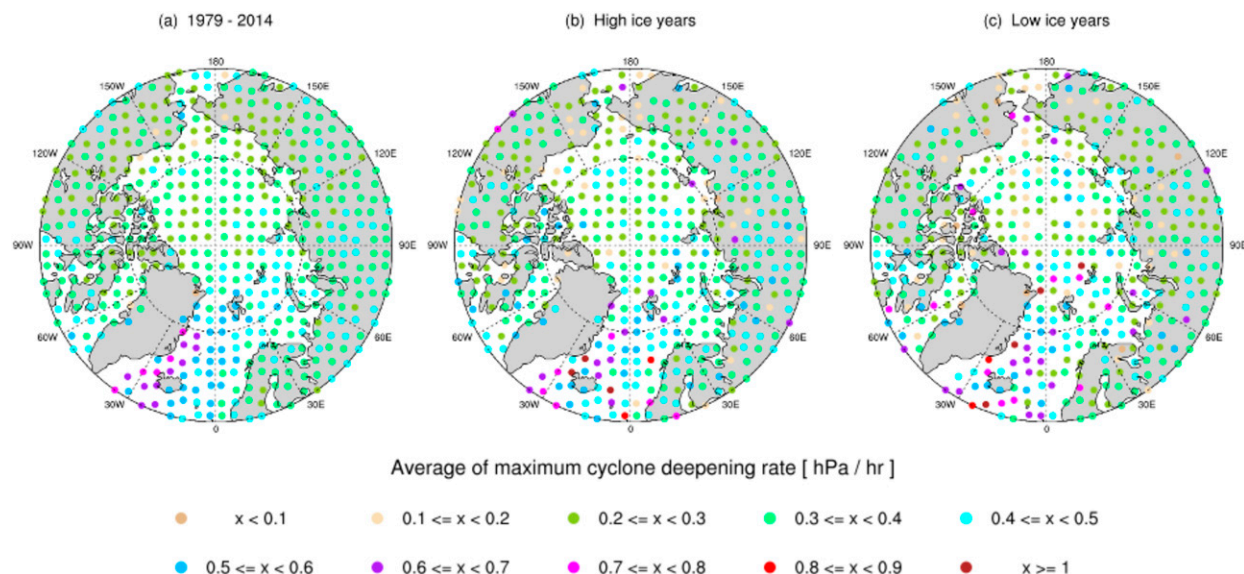
FIG. 9. Average of maximum cyclone deepening rates derived from NCEP–NCAR reanalysis, (a) from 1979 to 2014, during (b) +1.0 SD high and (c) −1.0 SD low ice years.

Arctic-wide regions are 0.52 ($p = 0.001$) and 0.47 ($p = 0.004$), respectively. This suggests that when the AO index is positive, there is an increase in baroclinicity, increasing cyclogenesis, and the number of extreme cyclones in the Arctic. Thus, the AO constitutes part of the decadal-scale variability in extreme cyclones, particularly in the GNB region but also on a pan-Arctic scale. However, several studies have suggested that the relationship between the North Atlantic Oscillation (NAO) (Hurrell et al. 2003) index and other climatic variables such as SLP, SST, or surface air temperature is not stationary in time (e.g., Rogers 1997; Zveryaev 1999; Polyakova et al. 2006; Haylock et al. 2007). Thus, if there is strong interdecadal variability in the relationship between the DJF AO index and extreme cyclone counts, it is possible that those coefficients can be varied by the length of study period.

Nevertheless, extreme cyclone frequency differences between low and high ice years are statistically significant ($p \leq 0.01$) from paired t tests, with positive differences in the vicinity of the Aleutian Islands for all periods and within the Barents Sea and North Atlantic during the pentad and ±1.0 SD composites combined with negative differences within the North Pacific Ocean and the Greenland, Norwegian, Barents, and Kara Seas (Fig. 14). Further, there appears to be a westward shift in extreme cyclones in the North Pacific Ocean, while a northward progression in the North Atlantic is less certain. Small areas near Svalbard and south of Iceland during the pentad and ±1.0 SD period show increases in extreme cyclones, as well as near

Iceland during the last decade, but other regions show reductions.

8. Summary and discussion

To study whether or not a linkage between sea ice loss and cyclone activity has already emerged in the Arctic, we evaluated several metrics relevant to cyclones over the period 1979 to 2014. Cyclones are influenced by many factors, including land–sea temperature contrasts, local topography, near-surface temperature and specific humidity, and large-scale transient eddies leading to climate patterns such as the AO. The reduced spatial extent of Arctic sea ice (Fig. 2) impacts the heat and moisture
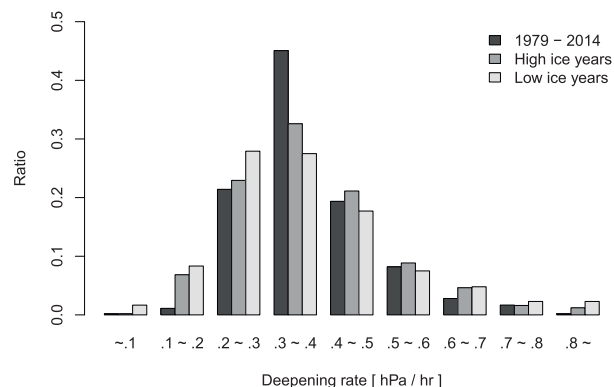

FIG. 10. Frequency of averaged maximum cyclone deepening rates derived from NCEP–NCAR reanalysis, from 1979 to 2014, and during high and low ice years.

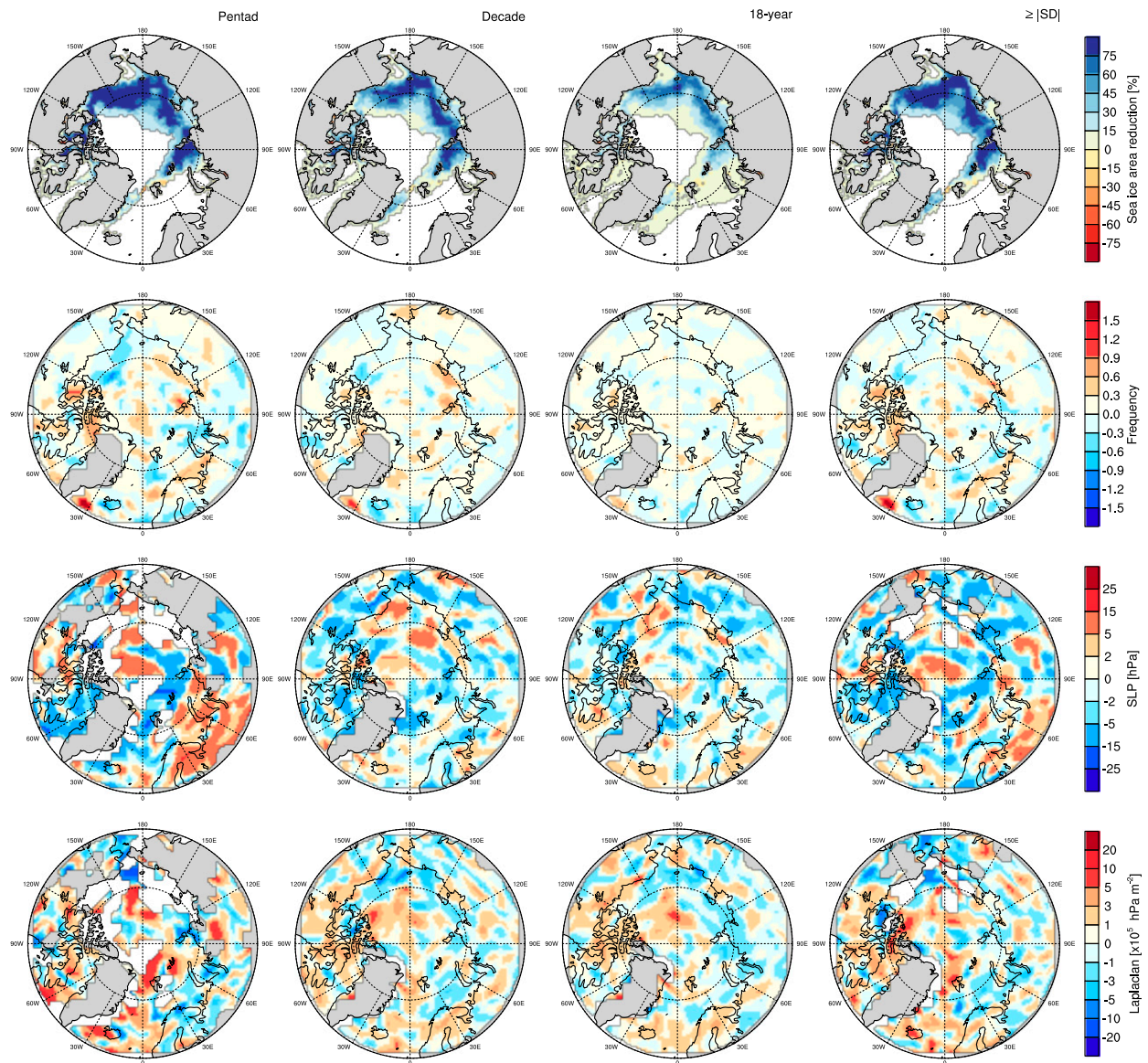## Difference in SON: "Low ice years" minus "High ice years"

FIG. 11. The temporal and spatial resolution of NCEP–NCAR reanalysis is 6-hourly on a 2.5° × 2.5° global grid, respectively. (from top to bottom) Composite September sea ice area change ratio from the high ice years to low ice periods; mean cyclone frequency from NCEP–NCAR; cyclone center mean SLPs from NCEP–NCAR; and cyclone center mean Laplacian from NCEP–NCAR. Each column period is the same as Fig. 4.

content of the overlying atmosphere, and can therefore potentially influence atmospheric circulation patterns and impact storm frequency and intensity. The combined changes of cyclones and SIE may have a significant impact not only on the Arctic ecosystem but also human activity. For example, strong winds from extreme cyclones produce storm surges and extensive wave action, especially as fetch (distance to the ice edge) has grown in the coastal areas of the Beaufort, Chukchi, East Siberian,

Laptev, and Kara Seas (Fig. 4, row 1). Consequently, storms can cause disastrous damage to local communities as well as erosion and flooding. Thus, assessing how cyclone frequency and intensity will change under an Arctic with less sea ice is important for long-range planning.

To gain insight, we first examined heat exchange processes at the surface in response to sea ice loss. Enhanced turbulent heat fluxes and longwave radiation in autumn and winter from sea ice loss have reduced the

Difference in SON: "Low ice years" minus "High ice years"
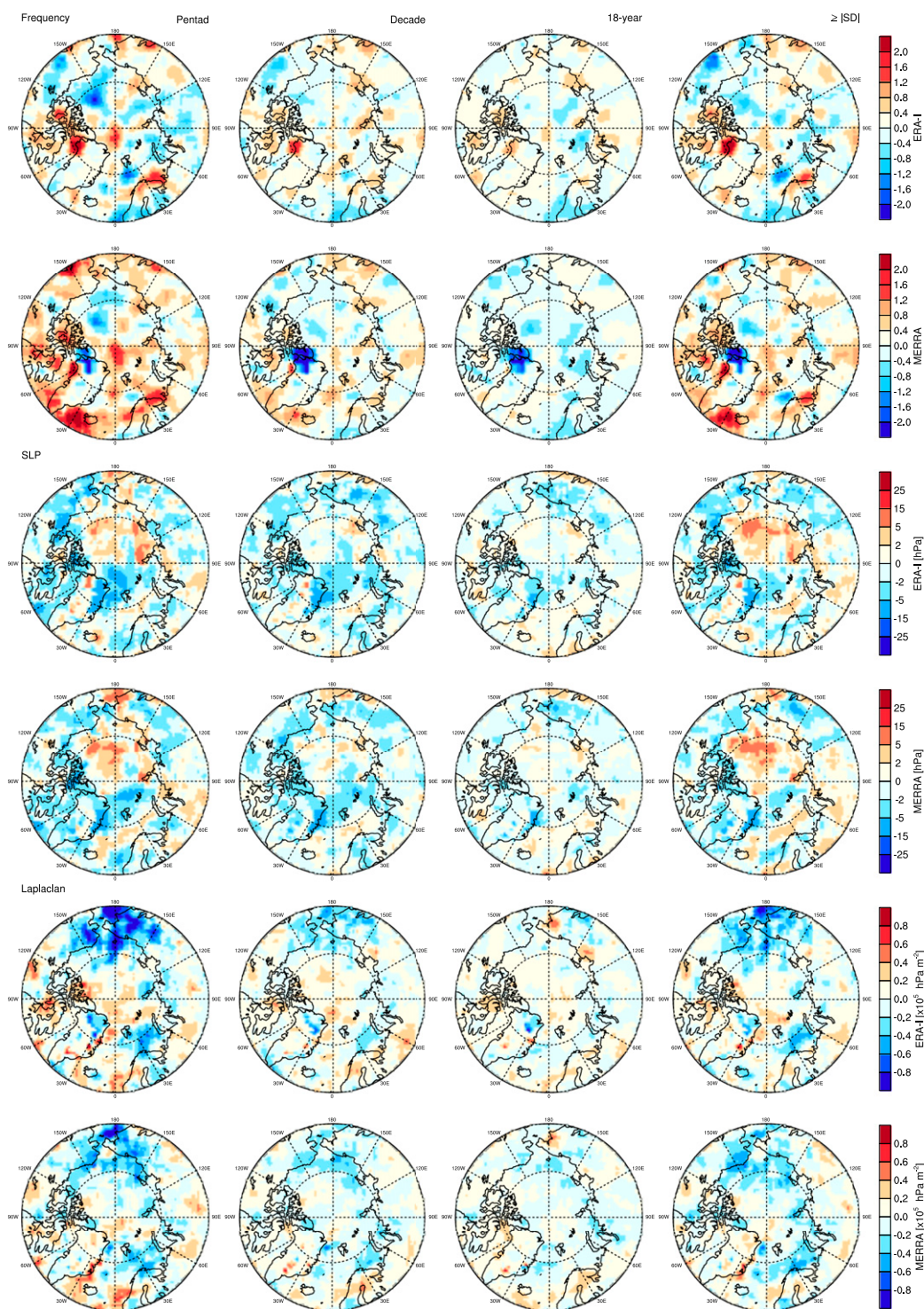
FIG. 12. The temporal and spatial resolution is 6-hourly on a 100 km × 100 km global grid, respectively. (from top to bottom) Mean cyclone frequency differences derived from ERA-Interim between the high ice years to low ice periods; as in row 1, but derived from MERRA; cyclone center mean SLPs differences derived from ERA-Interim between the high ice years to low ice periods; as in row 3, but derived from MERRA; cyclone center mean Laplacian differences derived from ERA-Interim between the high ice years to low ice periods; and as in row 5, but derived from MERRA. Each column period is the same as in Fig. 4.

(a) Extreme Cyclone Frequency   **(b) DJF Arctic Oscillation**
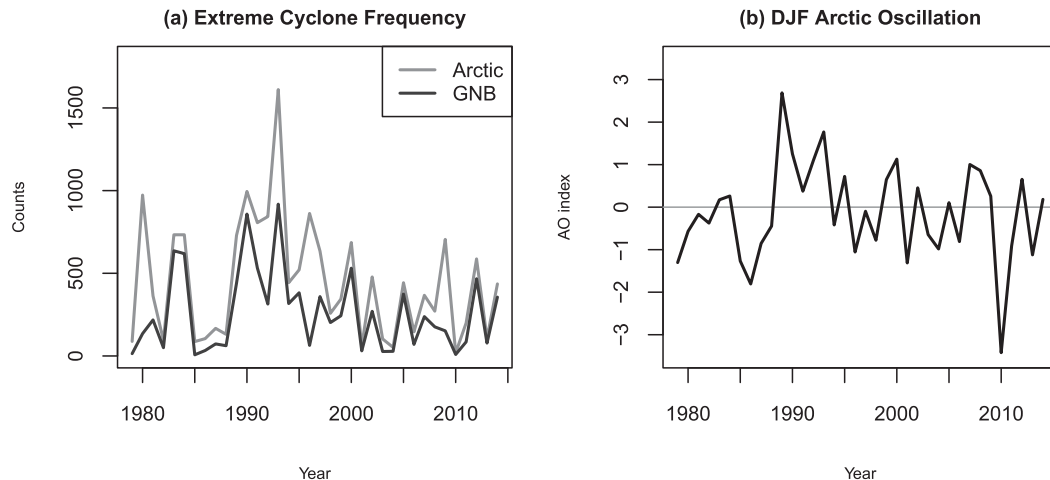
FIG. 13. Time series of (a) DJF extreme cyclone counts from NCEP–NCAR over GNB and the Arctic and (b) mean DJF Arctic Oscillation (AO) index.

atmospheric static stability (Fig. 4), as evidenced by increases in vertical temperature differences between 500 and 925 hPa (Fig. 5). A similar result has been found in other studies (e.g., Francis et al. 2009; Overland and Wang 2010; Stroeve et al. 2011; Jaiser et al. 2012). This has made the Arctic atmosphere more prone to baroclinic instability, which could in turn lead to more or stronger cyclones within the Arctic. Eady growth rate, which provides a measure of changes in the baroclinicity and the potential for cyclogenesis, further suggests that baroclinic instability over Greenland has increased as Arctic sea ice cover has decreased in autumn (Fig. 7). Combined, these results suggest an increased potential for cyclogenesis in the Arctic during low sea ice years.

In addition to the increased potential for cyclogenesis in the Arctic, expanding open water areas at the end of the melt season have led to substantial changes in moisture availability during subsequent months (Fig. 4), which may further increase the intensity of autumn and wintertime cyclones, and increase the amount of cyclone-associated precipitation, leading to increased snowfall. Yet it is important to note that changes in cyclone-associated precipitation do not necessarily *imply* a corresponding increase in cyclone intensity. Furthermore, Willison et al. (2013) suggest the response of cyclone intensity to atmospheric moisture increases may be a function of resolution of the reanalysis dataset.

While the observed atmospheric changes suggest the potential for increased cyclone activity and intensity, applying the Serreze et al. (1997) cyclone detection and tracking algorithm to the NCEP–NCAR atmospheric reanalysis does not suggest there has been an increase in autumn cyclone activity following years with low September SIE. On the other hand, results suggest that

cyclones are becoming stronger (as evaluated by the cyclone central SLP and local Laplacian) within limited areas: the northern Greenland, Norwegian, Barents, and Kara Seas (Fig. 11). Crawford and Serreze (2016) documented that the summer Arctic frontal zone, a narrow band of strong horizontal temperature gradients along the Arctic coastline, acts as an intensification area for systems forming over Eurasia. While the well-defined summer Eurasian frontal zone breaks down in autumn, frontal activity in the vicinity of Greenland is redeveloped (Serreze et al. 2001). Thus, it is hypothesized that the frontal activity from the Denmark Strait to Barents Sea is strengthened along with sea ice loss and acts as a modest intensifier of storms passing through the area in autumn. However, we find that intensification of cyclones is dependent on the choice of atmospheric reanalysis used, in agreement with previous studies (e.g., Raible et al. 2008; Ulbrich et al. 2009; Neu et al. 2013).

Finally, since a small change in the mean of a climate variable can result in a large change in the frequency of extremes (Mearns et al. 1984), extreme cyclones, identified as having anomalous deviation from a regionally mean SLP, were examined. Results suggest that DJF extreme cyclone tracks are shifted westward in the North Pacific Ocean while the frequency of extreme cyclones in the North Atlantic storm track has generally declined in response to sea ice loss (Fig. 14). This is counter to previous studies that have documented an increase in intensity and frequency of extreme Atlantic cyclones (Paciorek et al. 2002; Lehmann et al. 2011), and others that showed opposite trends in the eastern Pacific and North America (Gulev et al. 2001). Simmonds and Rudeva (2014) analyzed a subset of the most intense Arctic cyclones throughout the year using 10 different

Difference in DJF: mean counts of extreme cyclones

(a) Pentad

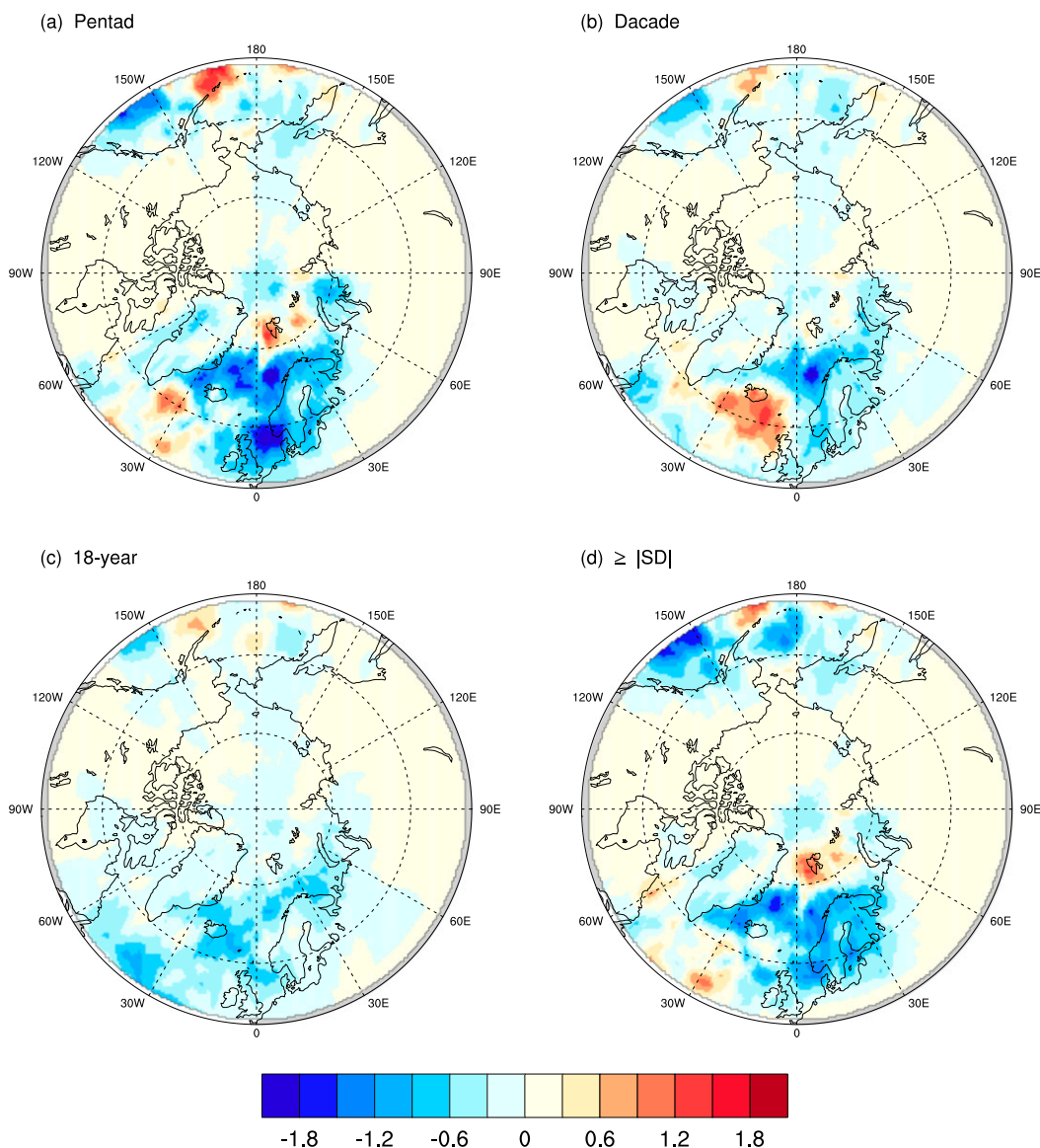(b) Dacade

(c) 18-year

(d) ≥ |SD|

FIG. 14. Extreme cyclone frequency difference in winter, low ice years minus high ice years.

cyclone-tracking algorithms and showed agreement among the algorithms as to location of the cyclone center. Thus, we have confidence that our results are robust. Romero and Emanuel (2017) suggest that while the annual number of North Atlantic polar lows will decline by 10%–15% in the future (2081–2100), a northward shift along the North Atlantic storm track is expected.

In summary, expanding open water areas in the Arctic have led to increased transfer of heat and moisture from the ocean to the atmosphere, warming and moistening the Arctic atmosphere and increasing the potential for cyclogenesis. However, a coherent change in autumn cyclone frequency has not yet been manifested despite evidence of a relationship between extreme cyclones and sea ice loss. This suggests that while there is some evidence that sea ice changes are impacting the potential for cyclogenesis; their effect on cyclone metrics is indistinct.

REFERENCES

Bengtsson, L., K. I. Hodges, and E. Roeckner, 2006: Storm tracks and climate change. *J. Climate*, **19**, 3518–3543, doi:10.1175/JCLI3815.1.

Boisvert, L. N., A. A. Petty, and J. C. Stroeve, 2016: The impact of the extreme winter 2015/16 Arctic cyclone on the Barents–Kara Seas. *Mon. Wea. Rev.*, **144**, 4279–4287, doi:10.1175/MWR-D-16-0234.1.

Boschat, G., I. Simmonds, A. Purich, T. Cowan, and A. B. Pezza, 2016: On the use of composite analyses to form physical hypotheses: An example from heat wave–SST associations. *Sci. Rep.*, **6**, 29599, doi:10.1038/srep29599.

Carnell, R. E., C. A. Senior, and J. F. B. Mitchell, 1996: An assessment of measures of storminess: Simulated changes in Northern Hemisphere winter due to increasing CO_2. *Climate Dyn.*, **12**, 467–476, doi:10.1007/s003820050121.

Cavalieri, D. J., C. L. Parkinson, P. Gloersen, J. C. Comiso, and H. J. Zwally, 1999: Deriving long-term time series of sea ice cover from satellite passive-microwave multisensor data sets. *J. Geophys. Res.*, **104**, 15 803–15 814, doi:10.1029/1999JC900081.

Chang, E. K. M., 2014: Impacts of background field removal on CMIP5 projected changes in Pacific winter cyclone activity. *J. Geophys. Res. Atmos.*, **119**, 4626–4639, doi:10.1002/2013JD020746.

——, Y. Guo, and X. Xia, 2012: CMIP5 multimodel ensemble projection of storm track change under global warming. *J. Geophys. Res.*, **117**, D23118, doi:10.1029/2012JD018578.

Charney, J. G., 1947: The dynamics of long waves in a baroclinic westerly current. *J. Meteor.*, **4**, 136–162, doi:10.1175/1520-0469(1947)004<0136:TDOLWI>2.0.CO;2.

Cohen, J. L., J. C. Furtado, M. A. Barlow, V. A. Alexeev, and J. E. Cherry, 2012: Arctic warming, increasing snow cover and widespread boreal winter cooling. *Environ. Res. Lett.*, **7**, 014007, doi:10.1088/1748-9326/7/1/014007.

Crawford, A. D., and M. C. Serreze, 2016: Does the summer Arctic frontal zone influence Arctic Ocean cyclone activity? *J. Climate*, **29**, 4977–4993, doi:10.1175/JCLI-D-15-0755.1.

Dee, D. P., and Coauthors, 2011: The ERA-Interim reanalysis: Configuration and performance of the data assimilation system. *Quart. J. Roy. Meteor. Soc.*, **137**, 553–597, doi:10.1002/qj.828.

de Jong, M. F., and L. de Steur, 2016: Strong winter cooling over the Irminger Sea in winter 2014–2015, exceptional deep convection, and the emergence of anomalously low SST. *Geophys. Res. Lett.*, **43**, 7106–7113, doi:10.1002/2016GL069596.

Descamps, L., D. Ricard, A. Joly, and P. Arbogast, 2007: Is a real cyclogenesis case explained by generalized linear baroclinic instability? *J. Atmos. Sci.*, **64**, 4287–4308, doi:10.1175/2007JAS2292.1.

Eady, E. T., 1949: Long waves and cyclone waves. *Tellus*, **1**, 33–52, doi:10.3402/tellusa.v1i3.8507.

Finnis, J., M. M. Holland, M. C. Serreze, and J. J. Cassano, 2007: Response of Northern Hemisphere extratropical cyclone activity and associated precipitation to climate change, as represented by the Community Climate System Model. *J. Geophys. Res.*, **112**, G04S42, doi:10.1029/2006JG000286.

Francis, J. A., W. Chan, D. J. Leathers, J. R. Miller, and D. E. Veron, 2009: Winter Northern Hemisphere weather patterns remember summer Arctic sea-ice extent. *Geophys. Res. Lett.*, **36**, L07503, doi:10.1029/2009GL037274.

Geng, Q., and M. Sugi, 2003: Possible change of extratropical cyclone activity due to enhanced greenhouse gases and sulfate aerosols—Study with a high-resolution AGCM. *J. Climate*, **16**, 2262–2274, doi:10.1175/1520-0442(2003)16<2262:PCOECA>2.0.CO;2.

Ghatak, D., A. Frei, G. Gong, J. Stroeve, and D. Robinson, 2010: On the emergence of an Arctic amplification signal in terrestrial Arctic snow extent. *J. Geophys. Res.*, **115**, D24105, doi:10.1029/2010JD014007.

——, C. Deser, A. Frei, G. Gong, A. Phillips, D. A. Robinson, and J. Stroeve, 2012: Simulated Siberian snow cover response to observed Arctic sea ice loss, 1979–2008. *J. Geophys. Res.*, **117**, D23108, doi:10.1029/2012JD018047.

Gitelman, A. I., J. S. Risbey, R. E. Kass, and R. D. Rosen, 1997: Trends in the surface meridional temperature gradient. *Geophys. Res. Lett.*, **24**, 1243–1246, doi:10.1029/97GL01154.

Gulev, S. K., O. Zolina, and S. Grigoriev, 2001: Extratropical cyclone variability in the Northern Hemisphere winter from the NCEP/NCAR reanalysis data. *Climate Dyn.*, **17**, 795–809, doi:10.1007/s003820000145.

Hall, N. M. J., B. J. Hoskins, P. J. Valdes, and C. A. Senior, 1994: Storm tracks in a high-resolution GCM with doubled carbon dioxide. *Quart. J. Roy. Meteor. Soc.*, **120**, 1209–1230, doi:10.1002/qj.49712051905.

Haylock, M. R., P. D. Jones, R. J. Allan, and T. J. Ansell, 2007: Decadal changes in 1870–2004 Northern Hemisphere winter sea level pressure variability and its relationship with surface temperature. *J. Geophys. Res.*, **112**, D11103, doi:10.1029/2006JD007291.

Hoskins, B. J., and P. J. Valdes, 1990: On the existence of storm-tracks. *J. Atmos. Sci.*, **47**, 1854–1864, doi:10.1175/1520-0469(1990)047<1854:OTEOST>2.0.CO;2.

Hurrell, J. W., Y. Kushnir, G. Ottersen, and M. Visbeck, 2003: An overview of the North Atlantic Oscillation. *The North Atlantic Oscillation: Climatic Significance and Environmental Impact, Geophys. Monogr.*, Vol. 134, Amer. Geophys. Union, 1–35, doi:10.1029/134GM01.

Inoue, J., and M. E. Hori, 2011: Arctic cyclogenesis at the marginal ice zone: A contributory mechanism for the temperature amplification? *Geophys. Res. Lett.*, **38**, L12502, doi:10.1029/2011GL047696.

——, ——, and K. Takaya, 2012: The role of Barents Sea ice in the wintertime cyclone track and emergence of a warm-Arctic cold-Siberian anomaly. *J. Climate*, **25**, 2561–2568, doi:10.1175/JCLI-D-11-00449.1.

Jaiser, R., K. Dethloff, D. Handorf, A. Rinke, and J. Cohen, 2012: Impact of sea ice cover changes on the Northern Hemisphere atmospheric winter circulation. *Tellus*, **64A**, 11595, doi:10.3402/tellusa.v64i0.11595.

Kalnay, E., and Coauthors, 1996: The NCEP/NCAR 40-Year Reanalysis Project. *Bull. Amer. Meteor. Soc.*, **77**, 437–471, doi:10.1175/1520-0477(1996)077<0437:TNYRP>2.0.CO;2.

Kuo, Y.-H., S. Low-Nam, and R. J. Reed, 1991: Effects of surface energy fluxes during the early development and rapid intensification stages of seven explosive cyclones in the western Atlantic. *Mon. Wea. Rev.*, **119**, 457–476, doi:10.1175/1520-0493(1991)119<0457:EOSEFD>2.0.CO;2.

Lee, W.-J., and M. Mak, 1994: Observed variability in the large-scale static stability. *J. Atmos. Sci.*, **51**, 2137–2144, doi:10.1175/1520-0469(1994)051<2137:OVITLS>2.0.CO;2.

Lehmann, A., K. Getzlaff, and J. Harlaß, 2011: Detailed assessment of climate variability in the Baltic Sea area for the period 1958 to 2009. *Climate Res.*, **46**, 185–196, doi:10.3354/cr00876.

Li, M., T. Woollings, K. Hodges, and G. Masato, 2014: Extratropical cyclones in a warmer, moister climate: A recent Atlantic analogue. *Geophys. Res. Lett.*, **41**, 8594–8601, doi:10.1002/2014GL062186.

Lim, E.-P., and I. Simmonds, 2007: Southern Hemisphere winter extratropical cyclone characteristics and vertical organization

observed with the ERA-40 data in 1979–2001. *J. Climate*, **20**, 2675–2690, doi:10.1175/JCLI4135.1.

Liu, J., J. A. Curry, H. Wang, M. Song, and R. M. Horton, 2012: Impact of declining Arctic sea ice on winter snowfall. *Proc. Natl. Acad. Sci. USA*, **109**, 4074–4079, doi:10.1073/pnas.1114910109.

McCabe, G. J., M. P. Clark, and M. C. Serreze, 2001: Trends in Northern Hemisphere surface cyclone frequency and intensity. *J. Climate*, **14**, 2763–2768, doi:10.1175/1520-0442(2001)014<2763:TINHSC>2.0.CO;2.

Mearns, L. O., R. W. Katz, and S. H. Schneider, 1984: Extreme high-temperature events: Changes in their probabilities with changes in mean temperature. *J. Climate Appl. Meteor.*, **23**, 1601–1613, doi:10.1175/1520-0450(1984)023<1601:EHTECI>2.0.CO;2.

Neu, U., and Coauthors, 2013: IMILAST: A community effort to intercompare extratropical cyclone detection and tracking algorithms. *Bull. Amer. Meteor. Soc.*, **94**, 529–547, doi:10.1175/BAMS-D-11-00154.1.

Noer, G., and M. Ovhed, 2003: Forecasting of polar lows in the Norwegian and the Barents Sea. *Proc. Ninth Meeting of the EGS Polar Lows Working Group*, Cambridge, United Kingdom, European Geophysical Society. [Available online at https://web.archive.org/web/20051122020825/https://www2.meteo.uni-bonn.de/mitarbeiter/GHeinemann/eplwg/newl03/noer/wplwg-2003-forecasting_polar_lows.html.]

Orsolini, Y. J., R. Senan, R. E. Benestad, and A. Melsom, 2012: Autumn atmospheric response to the 2007 low Arctic sea ice extent in coupled ocean–atmosphere hindcasts. *Climate Dyn.*, **38**, 2437–2448, doi:10.1007/s00382-011-1169-z.

Overland, J. E., and M. Wang, 2010: Large-scale atmospheric circulation changes are associated with the recent loss of Arctic sea ice. *Tellus*, **62A**, 1–9, doi:10.1111/j.1600-0870.2009.00421.x.

Paciorek, C. J., J. S. Risbey, V. Ventura, and R. D. Rosen, 2002: Multiple indices of Northern Hemisphere cyclone activity, winters 1949–99. *J. Climate*, **15**, 1573–1590, doi:10.1175/1520-0442(2002)015<1573:MIONHC>2.0.CO;2.

Parkinson, C. L., and J. C. Comiso, 2013: On the 2012 record low Arctic sea ice cover: Combined impact of preconditioning and an August storm. *Geophys. Res. Lett.*, **40**, 1356–1361, doi:10.1002/grl.50349.

Polyakova, E. I., A. G. Journel, I. V. Polyakov, and U. S. Bhatt, 2006: Changing relationship between the North Atlantic Oscillation and key North Atlantic climate parameters. *Geophys. Res. Lett.*, **33**, L03711, doi:10.1029/2005GL024573.

Raible, C. C., P. M. Della-Marta, C. Schwierz, H. Wernli, and R. Blender, 2008: Northern Hemisphere extratropical cyclones: A comparison of detection and tracking methods and different reanalyses. *Mon. Wea. Rev.*, **136**, 880–897, doi:10.1175/2007MWR2143.1.

Rasmussen, E., and J. Turner, 2003: *Polar Lows: Mesoscale Weather Systems in the Polar Regions*. Cambridge University Press, 612 pp.

Rienecker, M. M., and Coauthors, 2011: MERRA: NASA's Modern-Era Retrospective Analysis for Research and Applications. *J. Climate*, **24**, 3624–3648, doi:10.1175/JCLI-D-11-00015.1.

Rogers, J. C., 1997: North Atlantic storm track variability and its association to the North Atlantic Oscillation and climate variability of northern Europe. *J. Climate*, **10**, 1635–1647, doi:10.1175/1520-0442(1997)010<1635:NASTVA>2.0.CO;2.

Rogers, R. R., 1978: *Short Course in Cloud Physics*. 3rd ed. Butterworth-Heinemann, 304 pp.

Romero, R., and K. Emanuel, 2017: Climate change and hurricane-like extratropical cyclones: Projections for North Atlantic polar lows and medicanes based on CMIP5 models. *J. Climate*, **30**, 279–299, doi:10.1175/JCLI-D-16-0255.1.

Rudeva, I., S. K. Gulev, I. Simmonds, and N. Tilinina, 2014: The sensitivity of characteristics of cyclone activity to identification procedures in tracking algorithms. *Tellus*, **66A**, 24961, doi:10.3402/tellusa.v66.24961.

Screen, J. A., and I. Simmonds, 2010a: Increasing fall-winter energy loss from the Arctic Ocean and its role in Arctic temperature amplification. *Geophys. Res. Lett.*, **37**, L16707, doi:10.1029/2010GL044136.

——, and ——, 2010b: The central role of diminishing sea ice in recent Arctic temperature amplification. *Nature*, **464**, 1334–1337, doi:10.1038/nature09051.

Serreze, M. C., and A. J. Etringer, 2003: Precipitation characteristics of the Eurasian Arctic drainage system. *Int. J. Climatol.*, **23**, 1267–1291, doi:10.1002/joc.941.

——, and A. P. Barrett, 2008: The summer cyclone maximum over the central Arctic Ocean. *J. Climate*, **21**, 1048–1065, doi:10.1175/2007JCLI1810.1.

——, and R. G. Barry, 2014: *The Arctic Climate System*. 2nd ed. Cambridge University Press, 404 pp., doi:10.1017/CBO9781139583817.

——, and J. Stroeve, 2015: Arctic sea ice trends, variability and implications for seasonal ice forecasting. *Philos. Trans. Roy. Soc. London*, **373**, 20140159, doi:10.1098/rsta.2014.0159.

——, F. Carse, R. G. Barry, and J. C. Rogers, 1997: Icelandic low cyclone activity: Climatological features, linkages with the NAO, and relationships with recent changes in the Northern Hemisphere circulation. *J. Climate*, **10**, 453–464, doi:10.1175/1520-0442(1997)010<0453:ILCACF>2.0.CO;2.

——, A. H. Lynch, and M. P. Clark, 2001: The Arctic frontal zone as seen in the NCEP–NCAR reanalysis. *J. Climate*, **14**, 1550–1567, doi:10.1175/1520-0442(2001)014<1550:TAFZAS>2.0.CO;2.

——, A. P. Barrett, J. C. Stroeve, D. N. Kindig, and M. M. Holland, 2009: The emergence of surface-based Arctic amplification. *Cryosphere*, **3**, 11–19, doi:10.5194/tc-3-11-2009.

——, ——, and ——, 2012: Recent changes in tropospheric water vapor over the Arctic as assessed from radiosondes and atmospheric reanalyses. *J. Geophys. Res.*, **117**, D10104, doi:10.1029/2011JD017421.

Simmonds, I., 2015: Comparing and contrasting the behaviour of Arctic and Antarctic sea ice over the 35 year period 1979–2013. *Ann. Glaciol.*, **56**, 18–28, doi:10.3189/2015AoG69A909.

——, and K. Keay, 2009: Extraordinary September Arctic sea ice reductions and their relationships with storm behavior over 1979–2008. *Geophys. Res. Lett.*, **36**, L19715, doi:10.1029/2009GL039810.

——, and E.-P. Lim, 2009: Biases in the calculation of Southern Hemisphere mean baroclinic eddy growth rate. *Geophys. Res. Lett.*, **36**, L01707, doi:10.1029/2008GL036320.

——, and I. Rudeva, 2012: The great Arctic cyclone of August 2012. *Geophys. Res. Lett.*, **39**, L23709, doi:10.1029/2012GL054259.

——, and ——, 2014: A comparison of tracking methods for extreme cyclones in the Arctic basin. *Tellus*, **66A**, 25252, doi:10.3402/tellusa.v66.25252.

——, K. Keay, and E.-P. Lim, 2003: Synoptic activity in the seas around Antarctica. *Mon. Wea. Rev.*, **131**, 272–288, doi:10.1175/1520-0493(2003)131<0272:SAITSA>2.0.CO;2.

——, C. Burke, and K. Keay, 2008: Arctic climate change as manifest in cyclone behavior. *J. Climate*, **21**, 5777–5796, doi:10.1175/2008JCLI2366.1.

Sorokina, S. A., C. Li, J. J. Wettstein, and N. G. Kvamstø, 2016: Observed atmospheric coupling between Barents Sea ice and the warm-Arctic cold-Siberian anomaly pattern. *J. Climate*, **29**, 495–511, doi:10.1175/JCLI-D-15-0046.1.

Sorteberg, A., and J. E. Walsh, 2008: Seasonal cyclone variability at 70°N and its impact on moisture transport into the Arctic. *Tellus*, **60A**, 570–586, doi:10.1111/j.1600-0870.2008.00314.x.

Stramler, K., A. D. Del Genio, and W. B. Rossow, 2011: Synoptically driven Arctic winter states. *J. Climate*, **24**, 1747–1762, doi:10.1175/2010JCLI3817.1.

Stroeve, J. C., M. C. Serreze, A. Barrett, and D. N. Kindig, 2011: Attribution of recent changes in autumn cyclone associated precipitation in the Arctic. *Tellus*, **63A**, 653–663, doi:10.1111/j.1600-0870.2011.00515.x.

——, ——, M. M. Holland, J. E. Kay, J. Malanik, and A. P. Barrett, 2012: The Arctic's rapidly shrinking sea ice cover: A research synthesis. *Climatic Change*, **110**, 1005–1027, doi:10.1007/s10584-011-0101-1.

Sun, L., J. Perlwitz, and M. Hoerling, 2016: What caused the recent "warm Arctic, cold continents" trend pattern in winter temperatures? *Geophys. Res. Lett.*, **43**, 5345–5352, doi:10.1002/2016GL069024.

Tang, Q., X. Zhang, X. Yang, and J. A. Francis, 2013: Cold winter extremes in northern continents linked to Arctic sea ice loss. *Environ. Res. Lett.*, **8**, 014036, doi:10.1088/1748-9326/8/1/014036.

Thompson, D. W. J., and J. M. Wallace, 1998: The Arctic oscillation signature in the wintertime geopotential height and temperature fields. *Geophys. Res. Lett.*, **25**, 1297–1300, doi:10.1029/98GL00950.

Tsukernik, M., D. N. Kindig, and M. C. Serreze, 2007: Characteristics of winter cyclone activity in the northern North Atlantic: Insights from observations and regional modeling. *J. Geophys. Res.*, **112**, D03101, doi:10.1029/2006JD007184.

Ulbrich, U., G. C. Leckebusch, and J. G. Pinto, 2009: Extra-tropical cyclones in the present and future climate: A review. *Theor. Appl. Climatol.*, **96**, 117–131, doi:10.1007/s00704-008-0083-8.

Vallis, G. K., 2006: *Atmospheric and Oceanic Fluid Dynamics*. Cambridge University Press, 745 pp.

Vavrus, S. J., 2013: Extreme Arctic cyclones in CMIP5 historical simulations. *Geophys. Res. Lett.*, **40**, 6208–6212, doi:10.1002/2013GL058161.

Wallace, J. M., and P. V. Hobbs, 2006: *Atmospheric Science: An Introductory Survey*. 2nd ed. Vol. 92, International Geophysics Series, Academic Press, 504 pp.

Wang, X. L., V. R. Swail, and F. W. Zwiers, 2006: Climatology and changes of extratropical cyclone activity: Comparison of ERA-40 with NCEP–NCAR reanalysis for 1958–2001. *J. Climate*, **19**, 3145–3166, doi:10.1175/JCLI3781.1.

Willison, J., W. A. Robinson, and G. M. Lackmann, 2013: The importance of resolving mesoscale latent heating in the North Atlantic storm track. *J. Atmos. Sci.*, **70**, 2234–2250, doi:10.1175/JAS-D-12-0226.1.

Woods, C., and R. Caballero, 2016: The role of moist intrusions in winter Arctic warming and sea ice decline. *J. Climate*, **29**, 4473–4485, doi:10.1175/JCLI-D-15-0773.1.

Woollings, T., B. Harvey, M. Zahn, and L. Shaffrey, 2012: On the role of the ocean in projected atmospheric stability changes in the Atlantic polar low region. *Geophys. Res. Lett.*, **39**, L24802, doi:10.1029/2012GL054016.

Yamazaki, A., J. Inoue, K. Dethloff, M. Maturilli, and G. König-Langlo, 2015: Impact of radiosonde observations on forecasting summertime Arctic cyclone formation. *J. Geophys. Res. Atmos.*, **120**, 3249–3273, doi:10.1002/2014JD022925.

Zahn, M., and H. von Storch, 2010: Decreased frequency of North Atlantic polar lows associated with future climate warming. *Nature*, **467**, 309–312, doi:10.1038/nature09388.

Zhang, J., R. Lindsay, A. Schweiger, and M. Steele, 2013: The impact of an intense summer cyclone on 2012 Arctic sea ice retreat. *Geophys. Res. Lett.*, **40**, 720–726, doi:10.1002/grl.50190.

Zhang, X., J. E. Walsh, J. Zhang, U. S. Bhatt, and M. Ikeda, 2004: Climatology and interannual variability of Arctic cyclone activity: 1948–2002. *J. Climate*, **17**, 2300–2317, doi:10.1175/1520-0442(2004)017<2300:CAIVOA>2.0.CO;2.

Zveryaev, I. I., 1999: Decadal and longer changes of the winter sea level pressure fields and related synoptic activity over the North Atlantic. *Int. J. Climatol.*, **19**, 1177–1185, doi:10.1002/(SICI)1097-0088(199909)19:11<1177::AID-JOC424>3.0.CO;2-4.